# Enhancing the Catalysis for Electrochemical Water Splitting using Tri-metallic Phosphide Surface

Wenjie Liang[1], Lisi Yin[1], Yilin Zhou[1], Pan Yuan[1], Dan Wu[1], Xuehan Yang[1] and Tao Yang[1,*]

[1]*School of Environmental and Chemical Engineering, Jiangsu Ocean University, Lianyungang 222005 (China)*

**Abstract:** Hydrogen has been considered as one of the sustainable energy carriers and displays great potential for the ever-increasing energy and environmental demands. Electrochemical water splitting has been recognized as a clean and effective method to product hydrogen in future. Transitionally, the catalysts for water splitting are noble metal base materials but suffer from high cost and low reserves. Thus, developing cost-effective electrocatalysts is significantly important for the hydrogen generation. Here, we report a tri-metallic phosphide of NiCoFe-P as an effective electrocatalyst for both HER and OER, which can be prepared by a facile gas-phase reaction. Compared with monometallic or bimetallic phosphides, the tri-metallic NiCoFe-P exhibits outstanding activity. Specially, it obtains an OER current density of 10 mA $cm^{-2}$ at an overpotential of 248 mV. Additionally, the NiCoFe-P catalyst shows remarkable stabilities even at a large current density of 50 mA $cm^{-2}$. Moreover, a practical electrode of carbon paper supported NiCoFe-P only requires an overpotential of 267 mV to obtain an HER current density of 10 mA $cm^{-2}$, and overpotentials of 235 mV and 296 mV for the OER current densities of 50 mA $cm^{-2}$ and 100 mA $cm^{-2}$, respectively. After a severe durability test of 5000 cycles of linear scan voltammetry, the carbon paper supported catalyst show no degradation. The remarkable catalytic performance should be due to the unique nanostructure and the synergism effect among the hetero-atoms.

**Keywords**: Hydrogen evolution reaction, Oxygen evolution reaction, Porous nanostructure, Metal-organic frameworks, Overall water splitting, Metallic phosphide.

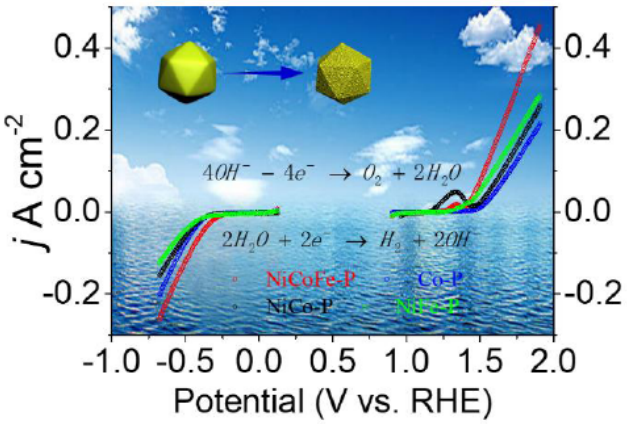


## 1. INTRODUCTION

Nowadays, it is critical to develop sustainable and clean substitution for fossil fuels [1]. Hydrogen is considered as one of the most potential energy carriers due to its high energy density and carbon-free features [2-5]. Accordingly, electrochemical water splitting has stood out to be a competitive way to produce high-purity hydrogen with carbon-free emissions from water [6-8]. Hydrogen and oxygen evolution are the two key reactions in water splitting. Transitionally, noble metal-based functional materials such as Pt, Ir and Ru, possess good catalytic activity for water splitting [9-13], however, the high price and rare reserves hinder their wide application. Therefore, it is imperative to develop cheap and efficient alternative electro-catalytic materials [14-17].

Recently, some transitional metal base materials show comparable or even better catalytic activities for water splitting [18-31], such as $CoS_2$ [32-39], CoP [40-45], $FeS_2$ [46-47], $Ni_2S_3$ [47, 48], $Ni_2P$ [49-51] and FeP [52-54]. Transition metal phosphides (TMPs) have been extensively investigated as low cost and high-performance electro-catalysts for HER in acid and alkaline solutions [55, 56]. In addition, the metal phosphides are also OER active in alkaline electrolyte

*Address correspondence to this author at the School of Environmental and Chemical Engineering, Jiangsu Ocean University, Lianyungang 222005 (China); E-mail: yangtao_hit@163.com

E-ISSN: 2410-4701/23 

because that metal phosphides would be partially oxidized to corresponding metal oxide or (oxy)hydroxides during catalyzing OER and form unique hetero-interface [57, 58]. Therefore, the metal phosphides are possible to be used as catalysts for overall water splitting in alkaline electrolyte [59, 60]. However, the electrical conductivity and the number of active sites of the mono-metallic compounds are below expectations. To overcome these issues, heteroatom compounds with two or three metal elements were developed [46, 47, 61-71]. Due to the difference in electronic structure and valence state, the electronic conductivity and the surface properties of the catalysts will be greatly improved [66, 68, 72, 73]. For example, the heteroatom of Fe can bring additional structural-vacancies and promote the electrochemical reactions on Ni [21]. In a nano-interface engineered $NiCo_2P_x$ system, Ni can synergistically facilitate water dissociation while Co can speed up the process of $H_2$ generation and release [7]. Recently, Yamauchi *et al*. reported a quaternary FeCoNiP hollow porous nanocube catalyst (100-200 nm), which showed an over-potential of 273 mV to achieve a current density of 10 mA $cm^{-2}$ for OER in an alkaline electrolyte [74]. This over-potential is lower than the reported NiCoP (280 mV) [75], CoP film (345 mV) [76], $Ni_5P_4$ films (290 mV) [49] and FeP (350 mV) [77], suggesting the positive effect of heteroatoms. However, this over-potential is still far below satisfaction.

Besides the influence of chemical compositions, the accessibility of active sites and electrode geometry also affects the activity of a catalyst greatly. Hollow or porous structures with high porosity and desirable pore distribution have attracted ever-increasing concerns for water splitting. The hollow micro-/nanostructures can provide a large number of active sites on the internal/external surfaces and plentiful gas release channels [78-81]. Moreover, a lot of optimized three-phase interface (hydrogen/oxygen, water, catalyst) can be produced in these micro-/nanoporous structures, which are important for HER and OER. Recently, extensive efforts have been devoted to complex hollow structures with subtle internal architecture. Metal-organic frameworks (MOFs), a family of crystalline material inclusive of metal ions center coordinated with several organic ligands, have inspired considerable attention due to the superior properties of high porosity, flexible tunability and well-defined architecture [82-84]. Benefiting from the unique structural advantages, MOFs have been widely used as templates for the synthesis of functional nanomaterials, displaying promising prospects in energy conversion and storage applications [85-90]. The hollow or porous structural features can inherit to the following or the final products. Recently, Prussian blue analogue (PBA), a typical transition metal-organic framework, has emerged as the appealing precursors for the synthesis of three-dimensional nanostructured functional materials [30, 59, 91, 93].

Encouraged by these marked findings of chemical composition and structural improvements, we herein synthesized tri-metallic phosphide of NiCoFe-P. The present NiCoFe-P was synthesized through a PBA-template-assisted method and show polyhedron in shape with high porosity. Compared with monometallic and bimetallic phosphides, the tri-metallic FeCoNi-PS show remarkable enhancement for both HER and OER in the alkaline electrolyte of 1 M KOH solution. The carbon paper supported NiCoFe-P catalyst exhibits an overpotential of 235 mV for the OER current density of 50 mA $cm^{-2}$ and needs only 296 mV to obtain the large current density of 100 mA $cm^{-2}$. In the case of HER, the carbon paper supported NiCoFe-P requires 386 mV and 469 mV for the counterpart current densities. In addition, the NiCoFe-P catalyst shows excellent durability and long-term stability in alkaline electrolyte.

## 2. RESULTS AND DISCUSSION

The synthetic route for PBA and its derived porous phosphide is schematically illustrated in Scheme **1**. Tri-metallic PBA was synthesized through a modified

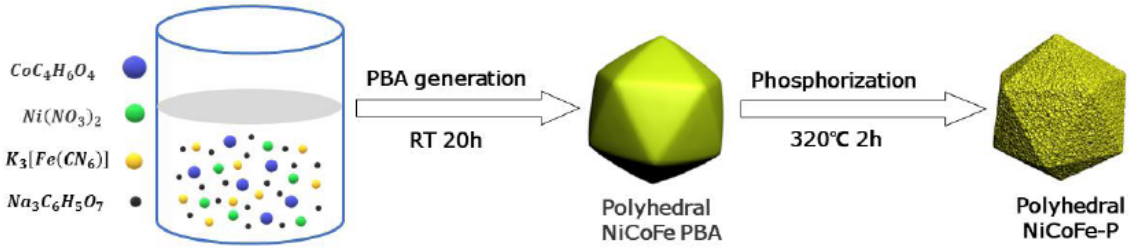


**Scheme 1:** Schematic illustration for the formation process of Porous NiCoFe-P polyhedrons.

precipitation process at room temperature (See Experimental Section) [78]. The XRD pattern (Figure **S1**) confirms the formation of the compounds of $K_2CoFe(CN)_6$, $K_2FeNi(CN)_6$ and $KNiFe(CN)_6$. Scanning electron microscopy (SEM) image in Figure **1a** shows that the as-produced NiCoFe PBAs are dominantly polyhedron in shape with smooth surfaces, distinct edges and corners. The polyhedral morphology can also be clearly observed by transmission electron microscopy (TEM) image in Figure **S2** (Supporting Information). The diameter of the polyhedron is in the range of 200-260 nm. The NiCoFe PBA was then phosphatized by reacting with $NaH_2PO_4{\cdot}2H_2O$ at 320 $^oC$ for 2 hr. Porous tri-metallic phosphide was then successfully produced.

SEM images in Figure **1b** and **1c** show that compared with the NiCoFe-PBA particles, the products still reserved as polyhedral shape and similar particle size but the surface became much rougher and porous. These structural features can be clearly demonstrated in the TEM image in Figure **1d**. High-resolution TEM (HRTEM) image in Figure **1e** shows that NiCoFe-P has lattice fringes with d-spacings of 2.09 and 2.50 Å, highly corresponding to the (112) plane of $FeNi_2P$ and (200) plane of $CoP_2$, suggesting the formation of transition metal phosphides. The chemical compositions of the product were demonstrated by TEM-EDS spectra (Figure **S3**), the atomic ratio of Fe, Co, Ni and P in the NiCoFe-P sample is ≈1.1:1:0.6:1.4, highly similar to the results from inductively coupled plasma-mass spectroscopy (ICP-MS) analysis. Morphology and the elemental distribution were further measured by Scanning transmission electron microscopy (STEM) test. HAADF-STEM image (Figure **1f**), the corresponding Energy-dispersive X-ray spectroscopy (EDS) elemental mapping (Figure **1h-k**), and the line-scanning profile (Figure **1g**) across an individual NiCoFe-P particle demonstrate that the elements of Ni, Co, Fe and P are homogeneously distributed on the particles.

For comparison, monometal and bimetal phosphides were also successfully synthesized through the same procedure (Figure **2**). XRD spectra demonstrate the formation of these PBA precursors

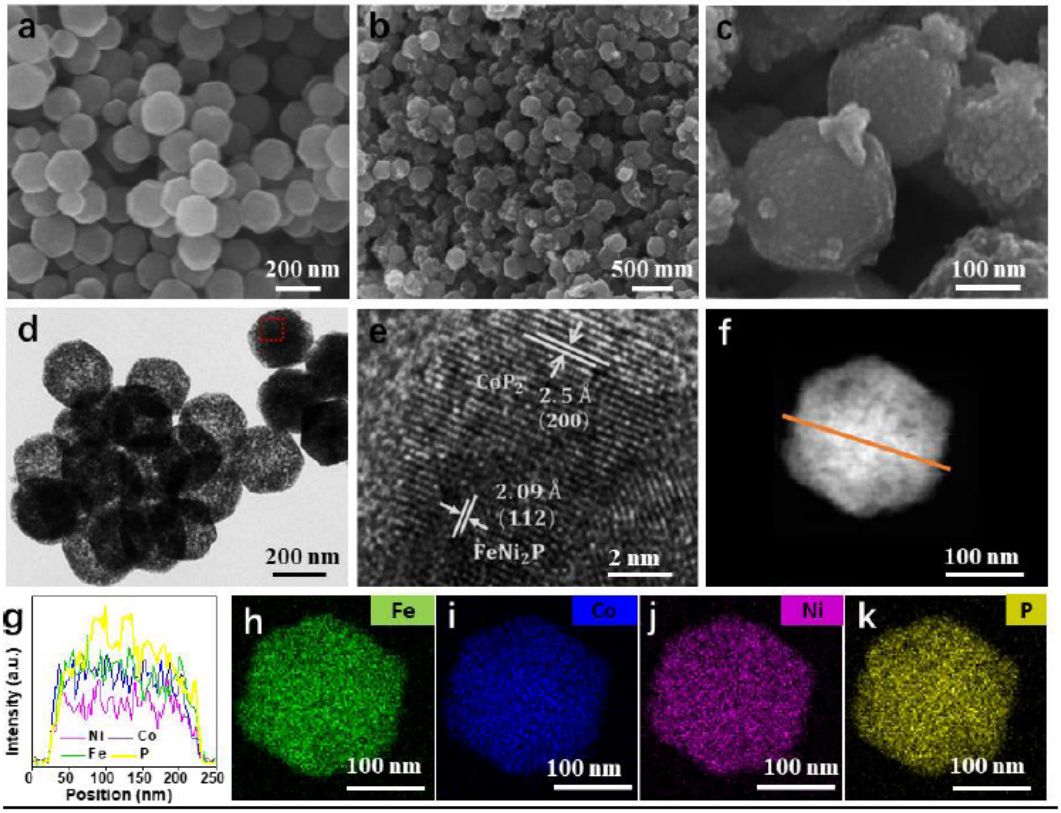


**Figure 1**: 第一个图重复Morphology and elemental distribution of the NiCoFe-P nanostructures. (**a**-**c**) Scanning electron microscopy (SEM) images of the prepared NiCoFe-PBA precursor, NiCoFe-P and magnification image of NiCoFe-P nanostructure. (**d**-**e**) Transmission electron microscopy (TEM) and High-resolution TEM (HRTEM) image of the NiCoFe-P nanostructure. (**f**) Scanning TEM (STEM) image. (**g**) Line-scanning profile of NiCoFe-P nanostructure and the corresponding elemental mapping of (**h**) Iron, (**i**) Cobalt, (**j**) Nickel, and (**k**) Phosphorus.

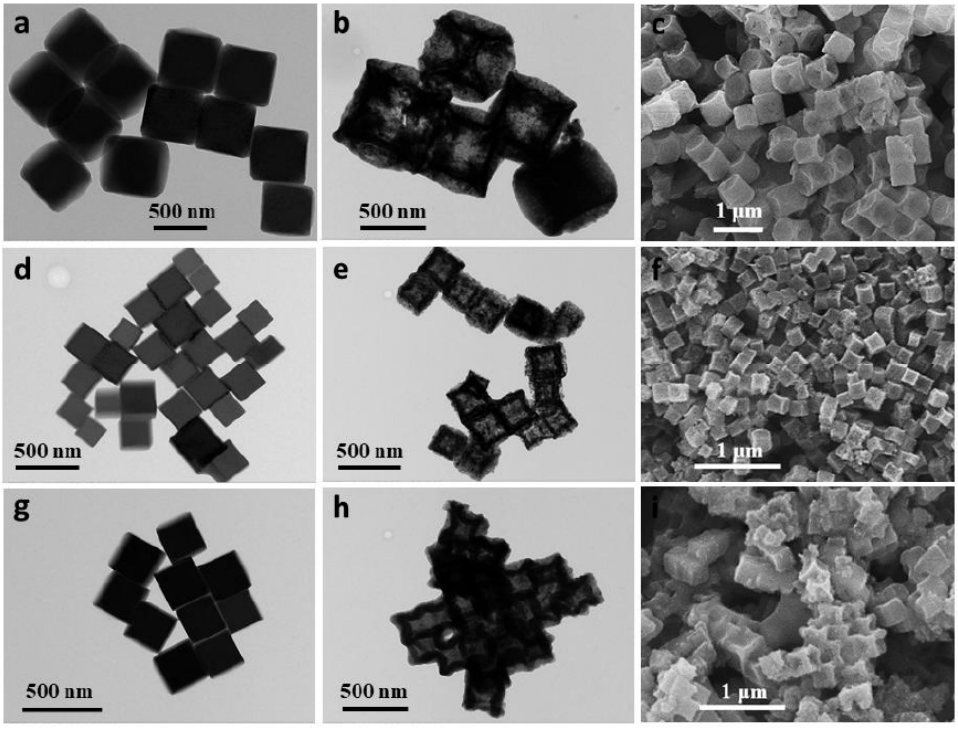


**Figure 2:** (**a**、**d** and **g**) TEM image of the NiCo PBA, CoCo PBA and NiFe PBA precursor, (**b**、**e** and **h**) TEM image of as-prepared NiCo-P, CoP and NiFe-P hollow nanocubes. (**c**、**f** and **i**) Typical SEM image of as-prepared NiCo-P, CoP and NiFe-P hollow nanocubes.

(Figure **S4**). It is interesting that these monometal and bimetal phosphides are cubic in shape with a hollowed interior structure, no matter chemical compositions and size. Compared with NiCoFe-P, these characteristics might be related to the absence of Fe, which needs further investigation. The Chemical compositions and the elemental distribution were tested by TEM-EDS and EDS elemental mapping (Figure **S5**-**8**), demonstrating the presence and uniform distribution of their elements.

The crystalline of the four phosphides was investigated by X-ray diffraction (XRD), the XRD patterns were shown in Figure **3**. In the XRD pattern of NiCoFe-P, the peak at 35.8° corresponds to the (200) plane of $CoP_2$, and the peak at 43.1° can be assigned to the (112) plane of $FeNi_2P$, the weak peak at 56.2° should be the (320) plane of $Co_2P$, while the peak at 62.6° should be attributed to the (321) plane of $NiP_2$. These results are good in agreement with the above HRTEM result, indicating that PBA can be successfully transferred to phosphides in our method. In the pattern of NiCo-P, the peak at 36.9° can be assigned to the (310) planes of $CoP_3$, and the diffractions of 40.9° and 43.0° are due to the (201) and (211) planes of $Co_2P$, the peaks at 44.5° and 54.9° should be attributed to the (201) and (211) planes of $Ni_2P$, while the peak at 62.3° corresponds to the (032) plane of $CoP_2$, and the peak at 74.7 should be the (400) plane of $Ni_2P$. For the diffraction of NiFe-P, the peaks at 37.2° and 62.9° correspond to the (210) and (321) planes of $NiP_2$, while the peaks at 36.9° and 43.4° can be assigned to the (301) and (112) planes of $FeNi_2P$, respectively. As to the pattern of Co-P, the peaks at 31.3°, 40.9° and 42.0° are attributed to the (120), (201) and (220) planes of $Co_2P$, respectively, the peaks at 36.9° and 59.4° should be assigned to the (310) plane of $CoP_3$ and the (131) plane of $CoP_2$, respectively.

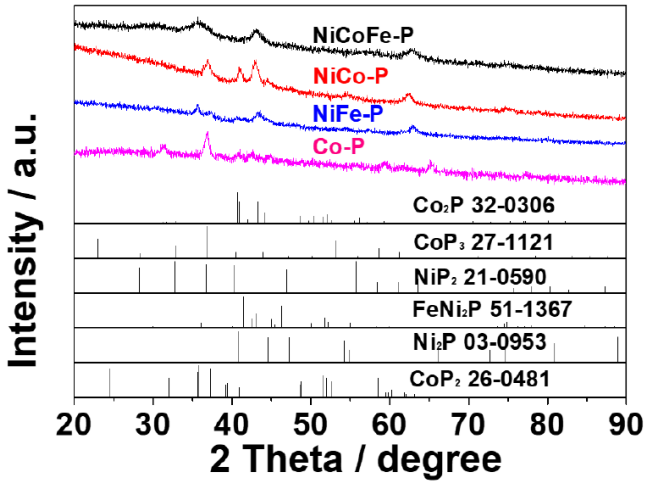


**Figure 3**: XRD profiles of as-prepared NiCo-P, CoP), NiFe-P and NiCoFe-P.

The chemical compositions and valence states of the elements on the NiCoFe-P, NiCo-P, NiFe-P and Co-P surfaces are characterized by X-ray photoelectron spectroscopy (XPS) detection. The survey spectra in Figure **S9** manifest the existence of Ni, Co, Fe and P, matching well with the above TEM-EDX results. Figure **4a** shows the high-resolution spectra of Ni for NiCoFe–P, the peak at ~854.5 eV can be attributed to $Ni^{\delta+}$ in the Ni-P compound and the peak at ~856.1 eV should be indexed to $Ni^{2+}$ in nickel oxide. Figure **4b** shows the high-resolution spectra of Fe, the peaks at 706.9 and 719.1 eV are corresponding to the Fe $2p_{2/3}$ and Fe $2p_{1/2}$ of the Fe-P bonds, respectively, while the peaks at 711.4 and 724.5 eV should be assigned to the Fe $2p_{2/3}$ and Fe $2p_{1/2}$ of the Fe-O bond on the surface, respectively, suggesting the formation of iron oxide. As to the spectra of Co in Figure **4c**, the small peaks at 778.5 eV and 791.1 eV should be attributed to Co $2p_{3/2}$, and Co $2p_{1/2}$, respectively. The peaks located at 781.1 eV (Co $2p_{3/2}$) and 797.2 eV (Co $2p_{1/2}$) suggest the coexistence of $Co^{3+}$ and $Co^{2+}$. The high-resolution spectra of P are shown in Figure **4d**, and the two peaks at 129.5 eV and 130.0 eV are the binding energy of P $2p_{1/2}$ and P $2p_{3/2}$, respectively. The peak located at 133.5 eV can be characterized as the P-O bond, indicating the oxidization of the surface in the air atmosphere. The above results demonstrate the successful conversion from PBA to phosphide via the low-temperature gas phosphatization process. The XPS spectra of NiCoFe–P are also compared with those of monometal and bimetal phosphides (Figure **S10**-**S13**). While there are some differences in the XPS spectra of Fe, Co and Ni among the tested materials. The reason for this might be due to the changing electronic environment resulting from different anions. It should be noted that the ratio of the peaks for phosphide and P-O is slightly smaller in NiCoFe–P than the counterparts in monometal and bimetal phosphides, suggesting the more oxidization on NiCoFe–P surface.

The electrochemical HER activity of NiCoFe-P was demonstrated in argon saturated 1.0 M KOH electrolyte in a typical three-electrode system. Glassy carbon electrode with 0.3 mg $cm^{-2}$ was used as the working electrode. Alkaline-efficient catalysts are of significant importance and attract more and more attention because that alkaline solution is the most widely used

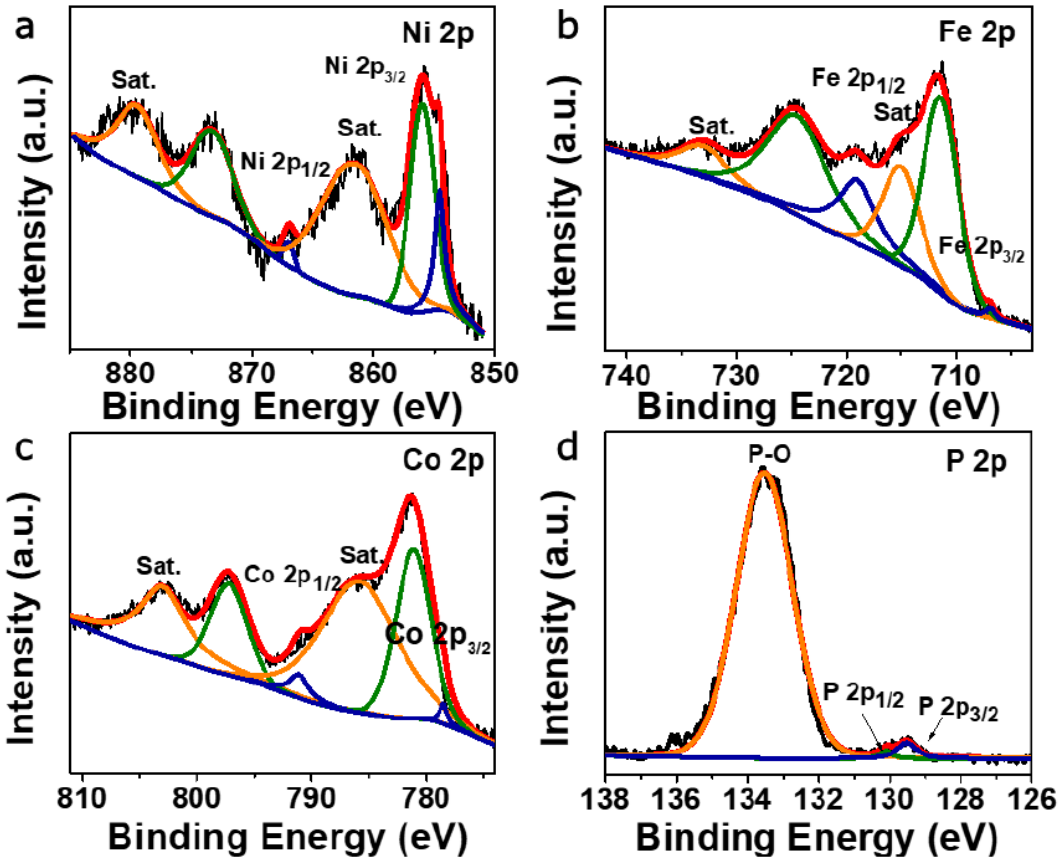


**Figure 4:** XPS spectrum of NiCoFe–P: High-resolution spectra of (**a**) Fe 2p, (**b**) Ni 2p, (**c**) Co 2p and (**d**) P 2p.

electrolyte in the industry. For comparison, Co-P, NiFe-P and NiCo-P catalysts were also tested under the same conditions. NiCoFe-P shows the smallest onset potential of -237 mV for the HER current density of 1 mA $cm^{-2}$, which is much lower than that of NiFe-P (-271 mV), not to mention those of Co-P (-350 mV) and NiCo-P (-368 mV), suggesting the much better catalytic performance of NiCoFe-P even at the very beginning. To achieve a current density of 10 mA $cm^{-2}$, the critical value for driving solar fuel conversion system, NiCoFe-P requires an overpotential of 350 mV, while NiFe-P, Co-P and NiCo-P need 431 mV, 463 mV and 511 mV respectively. To obtain a large current density of 50 mA $cm^{-2}$, NiCoFe-P requires an overpotential of 445 mV. The performance at large current density suggests a quite promising future for practical industry electrolysis applications. Tafel plot is employed to evaluate the efficiency of electrocatalysts (Figure **5c**). A smaller Tafel slop normally means that an electrocatalyst requires a smaller increment in overpotential to achieve the required current density. In this study, Tafel slops of NiCoFe-P is in the range of Volmer (118.2 mV $dec^{-1}$) and Heyrovsky (39.4 mV $dec^{-1}$), suggesting a Volmer-Heyrosky mechanism ($H_2O + e^- = H_{ads} + OH^-$ and $H_2O + e^- + H_{ads} = H_2 + OH^-$). While the other three samples show larger Tafel slop than 118.2 mV $dec^{-1}$, indicating a sluggish kinetics process. The stability of NiCoFe-P was tested by chronoamperometric responses (i-t) at a given overpotential of 350 mV. The catalyst preserved a current density of 10 mA $cm^{-2}$ after 10000 s. A more rigorous overpotential of 445 mV was then applied, the catalyst still showed excellent stability and preserved 96 % of its initial current density after 10000 s.

The electrochemical OER performance was also tested in a 1.0 M KOH solution in three electrodes system by positive polarizing. NiCoFe-P shows the highest catalytic performance, obtains an overpotential of 248 mV for the OER current density of 10 mA $cm^{-2}$, which is much smaller than the other controlled samples including Co-P (295 mV), NiCo-P (338 mV) and NiFe-P (306mV) (Figure **6b**). At larger current densities of 50 and 100 mA $cm^{-2}$, the NiCoFe-P need small overpotentials of 332 mV and 421 mV, respectively, much smaller than Co-P (397 and 487) and NIFe-P (415 and 522), not to mention NiCo-P (534 mV for 50 mA $cm^{-2}$). In addition, NiCoFe-P shows the smallest Tafel slope of 67 mV $dec^{-1}$, indicating the smallest increment in overpotential with the increase of current density, and in turn a remarkable performance

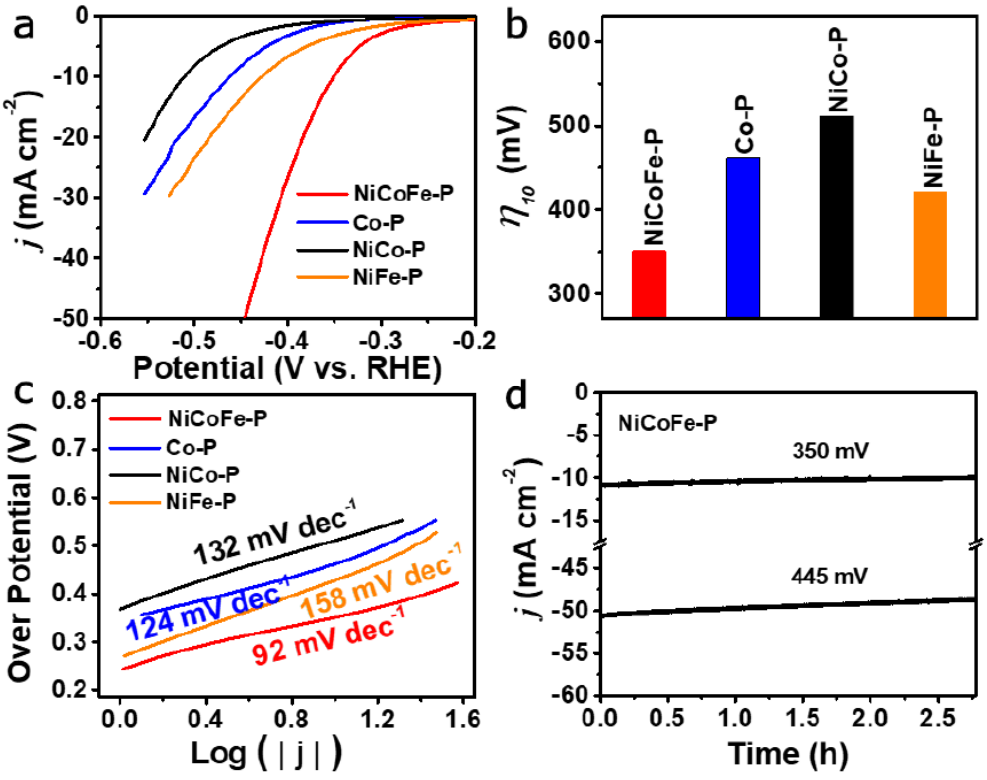


**Figure 5:** (**a**) Polarization curves, (**b**) the overpotentials for delivering the HER current density of 10 mA $cm^{-2}$, and (**c**) the corresponding Tafel plots of NiCoFe-P, Co-P, NiCo-P and NiFe-P for HER in 1 M KOH solution. (**d**) Chronoamperometric responses (*i–t*) collected on the NiCoFe-P at the applied overpotentials of 350 mV and 445 mV, respectively. All the polarization curves were collected without iR-correction.

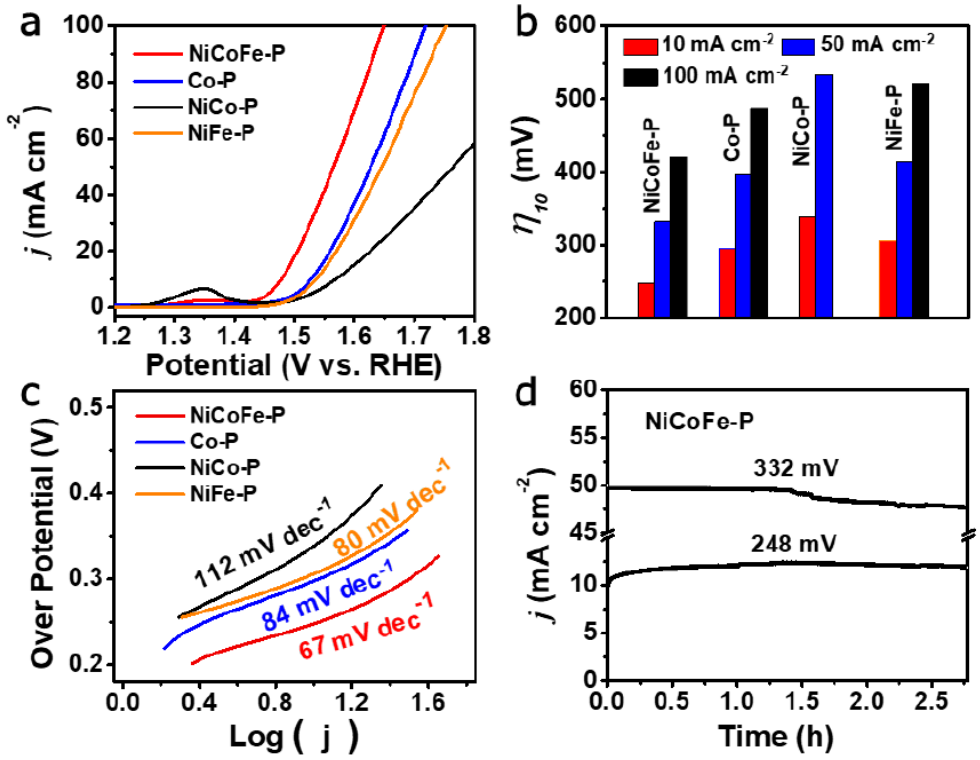


**Figure 6**: (**a**) Polarization curves, (**b**) the overpotentials for delivering the OER current density of 10 mA $cm^{-2}$, 50 mA $cm^{-2}$ and 100 mA $cm^{-2}$, respectively, and (**c**) the corresponding Tafel plots of the NiCoFe-P, Co-P, NiCo-P and NiFe-P for OER in 1 M KOH solution. (**d**) Chronoamperometric responses (*i–t*) collected on the NiCoFe-P at the applied overpotentials of 248 mV and 332 mV, respectively. All the polarization curves were collected without iR-correction.

at large current density region for water splitting. In accordance with the previous reports, the decreased overpotential for NiCoFe-P should be attributed to the synergistic effects of the different metal phosphides. In the heterometallic phosphide, Ni species serve as active sites, and the homogeneously distributed Fe and Co can tune the electronic properties of the active centers and thus improve the OER catalysis. The stability of NiCoFeP was tested through the chronoamperometric responses (*i-t*) at a given overpotential of 248 mV. As shown in Figure **5d**, the OER current density increased in the initial 1.5 h and still larger than 10 mA $cm^{-2}$ at 10000 s. The overpotential was then increased to 332 mV, corresponding to a current density of 50 mA $cm^{-2}$ at the beginning, 47.5 mA $cm^{-2}$ preserved after 10000 s. Another stability test was also conducted that NiCoFe-P underwent 2000 scans from 1.2 V to 1.7 V at a constant scan rate of 50 mV $s^{-1}$ (Figure **S14**). The LSV curve was then recorded, which exhibits negligible loss in comparison with the initial one. These results indicate that NiCoFe-P is superiorly durable for OER in alkaline electrolytes.

The above electrochemical measurements show that NiCoFe-P exhibits excellent catalytic activities for both HER and OER in alkaline electrolyte. The excellent performance should be attributed to the following features. i) First, Ni and Co compounds are active catalysts for OER, HER and overall water splitting, however, they usually show compromised performance due to the limited exposed metal active sites. The unique porous polyhedron structure of our NiCoFe-P with the rough and loose surface, inherited from PBA, providing and exposing more molecular metal centers as active sites, allows for sufficient contact between catalyst and electrolyte, and promotes rapid mass transfer and gas diffusion [94]. ii) Besides, the poor crystallinity of NiCoFe-P, evidenced by weak XRD spectra, could offer more unsaturated atoms as active sites [95], facilitating the adsorption of reactants in the active site, thus accelerating the reaction rate. iii) Furthermore, the modification of the electronic structure caused by the hetero-atoms of Fe, Co and Ni are beneficial for the proton-discharging process [96], which leads to an improvement for HER. It has also been reported that Fe and P can adjust the energy barrier of the reaction to an optimal value, and then promote the evolution of oxygen, thus enhances OER [97]. Meanwhile, the synergism effect among the hetero-atoms could reduce the charge transfer

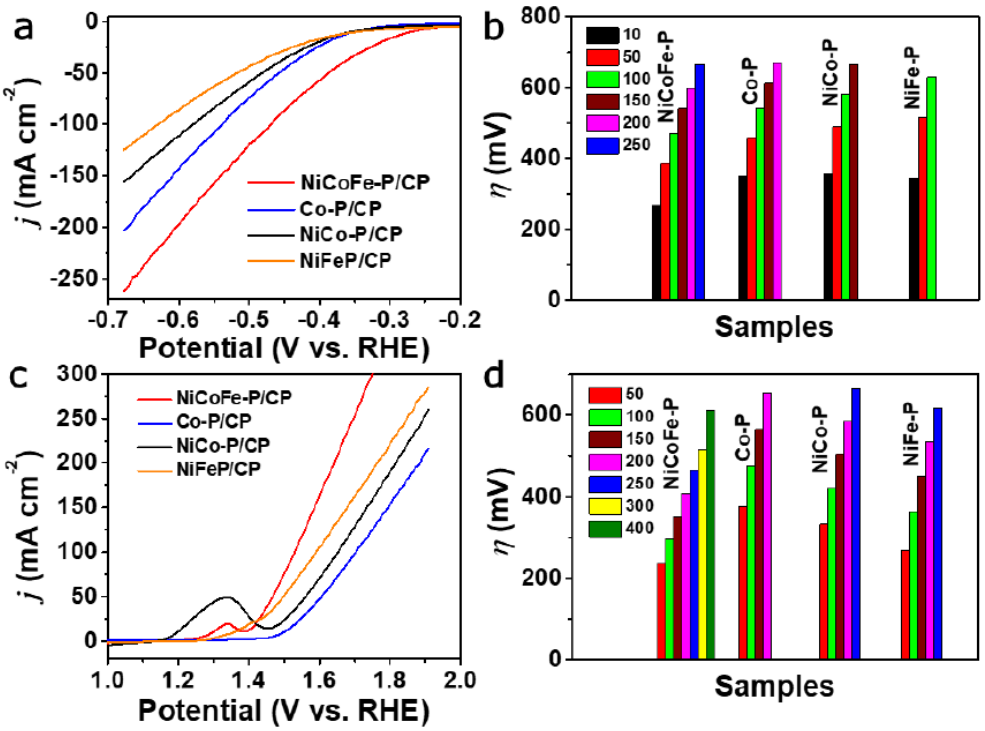


**Figure 7:** (**a**) Polarization curves and (**b**) the overpotentials of NiCoFe-P/CP, Co-P/CP, NiCo-P/CP and NiFe-P/CP for HER current densities of 10 mA $cm^{-2}$, 50 mA $cm^{-2}$, 100 mA $cm^{-2}$, 150 mA $cm^{-2}$, 200 mA $cm^{-2}$ and 250 mA $cm^{-2}$, respectively. (**c**) Polarization curves and (**d**) the overpotentials of NiCoFe-P/CP, Co-P/CP, NiCo-P/CP and NiFe-P/CP for OER current densities of 50 mA $cm^{-2}$, 100 mA $cm^{-2}$, 150 mA $cm^{-2}$, 200 mA $cm^{-2}$, 250 mA $cm^{-2}$, 300 mA $cm^{-2}$ and 400 mA $cm^{-2}$, respectively. All the polarization curves were collected without iR-correction. LSV scan rate: 5 mV $s^{-1}$ for HER and 10 mV $s^{-1}$ for OER.

resistance, resulting in faster electron transport and lower the overpotential for HER and OER [95]. In the hetero-atomic system, Ni can serve as the active sites for desorption of $OH^-$ (Volmer step) while Co serves as the active sites for the $H_{ads}$ recombination (Heyrovsky step) [71]. Fe can enhance the activity through the introduction of structural vacancies [21]. The electronic effect between the dangling P atom and H atoms can weaken the H-OH bond. With the aid of a free electron, the water molecule dissociates into an H atom on the dangling P atom and an $OH^-$ on the nearby Ni ion. The H atom then transfers onto a nearby vacant Co ion and becomes an adsorbed $H_{ads}$.

To emphasize the practical application and the performance for large current densities, the catalysts were loaded onto carbon paper (Carbon Paper Electrode, CPE) that has been usually used in water-splitting cells (see electrode preparation details in the Experimental Section). All the carbon paper supported catalysts achieve higher current density due to the larger loading amount (3 mg $cm^{-2}$), ten times higher than the RDE tests (0.3 mg $cm^{-2}$). In addition, the onset potential and overpotential for special current density reduced greatly. NiCoFe-P obtains a current density of 10 mA $cm^{-2}$ at an overpotential of 269 mV, much smaller than the overpotential on RDE for the same current density (351 mV). This reduction of overpotentials also happened to the catalysts in the OER test. NiCoFe-P loaded on RDE achieved 50 mA $cm^{-2}$ at an overpotential of 445 mV, while only required an overpotential of 386 mV for the same current density. In the two cases of HER and OER, NiCoFe-P still shows the best catalytic performance compared with Co-P, NiCo-P and NiFe-P catalysts. We then performed cyclic voltammetry at various scan speed to calculate the electrochemical double-layer capacitance ($C_{dl}$), which has been widely used to estimate the electrochemical active surface area (EASA) of catalysts (Figure **S15**, **S16**). The EASA sequence for HER is NiFe-P>NiCoFe-P>Co-P>NiCo-P, and for OER is NiCo-P>NiCoFe-P>NiFe-P>Co-P, which suggests that the EASA is not a critical factor for the catalytic performance. Stability was also tested by successive linear sweep voltammetry (LSV), NiCoFe-P on carbon paper shows a negligible loss after 5000 cycles in both HER and OER (Figure **S17**, **S18**). All of the above results demonstrate the excellent practical performance of the present porous NiCoFe-P catalyst in alkaline electrolyte.

## CONCLUSION

In summary, hetero-atomic transition metal phosphides NiCoFe-P were successfully prepared via a facile phosphating strategy. The as-prepared NiCoFe-P catalysts exhibit distinctive porous nanostructure with rough and loose surfaces. Electrochemical measurements demonstrate that the present NiCoFe-P exhibits excellent electrochemical activities and outstanding long-term stability for both HER and OER. The exceptional catalytic performance of NiCoFe-P for OER and HER should be due to the unique porous nanostructure and the synergism effect among the hetero-atoms.

## ASSOCIATED CONTENT

### Supporting Information

Supporting information is available inclusive of Structural characterization, SEM and TEM images, HADDF-STEM images, TEM-EDS spectra, XRD pattern, Polarization curves.

### Notes

The authors declare no competing financial interest.

## ACKNOWLEDGMENT

This work was financially supported by the Natural Science Foundation of Jiangsu Province (No.BK20201466), the “521” Project of Lianyungang (LYG06521202132), the China Postdoctoral Science Foundation (2021M691327), the Jiangsu Postdoctoral Science Foundation (2021K313C), the Postgraduate Research & Practice Innovation Program of Jiangsu Province (KYCX21_3138), the Key University Science Research Project of Jiangsu Province (No.19KJA430007), and the project funded by the Priority Academic Program Development of Jiangsu Higher Education Institutions (PAPD).

## REFERENCES

[1] P. De Luna, C. Hahn, D. Higgins, S. A. Jaffer, T. F. Jaramillo and E. H. Sargent, Science, 2019, 364, eaav3506. https://doi.org/10.1126/science.aav3506

[2] Q. Yun, Q. Lu, X. Zhang, C. Tan and H. Zhang, Angew Chem Int Ed Engl, 2018, 57, 626-646. https://doi.org/10.1002/anie.201706426

[3] B. Y. Xiong, L. S. Chen and J. L. Shi, ACS Catalysis, 2018, 8, 3688-3707. https://doi.org/10.1021/acscatal.7b04286

[4] H. A. Gasteiger and N. M. Marković, Science, 2009, 324, 48-49. https://doi.org/10.1126/science.1172083

[5] S. Mallapaty, Nature, 2020, 586, 482-483. https://doi.org/10.1038/d41586-020-02927-9

[6] Y. Zheng, Y. Jiao, M. Jaroniec and S. Z. Qiao, Angew. Chem. Int. Ed., 2015, 54, 52-65. https://doi.org/10.1002/anie.201407031

[7] D. R. Gamelin, Nat. Chem., 2012, 4, 965-967. https://doi.org/10.1038/nchem.1514

[8] Z.-Y. Yu, Y. Duan, X.-Y. Feng, X. Yu, M.-R. Gao and S.-H. Yu, Adv. Mater., 2021, 33, 2007100. https://doi.org/10.1002/adma.202007100

[9] C. C. L. McCrory, S. Jung, I. M. Ferrer, S. M. Chatman, J. C. Peters and T. F. Jaramillo, J. Am. Chem. Soc., 2015, 137, 4347-4357. https://doi.org/10.1021/ja510442p

[10] T. Reier, M. Oezaslan and P. Strasser, ACS Catal., 2012, 2, 1765-1772. https://doi.org/10.1021/cs3003098

[11] J. Wang, F. Xu, H. Jin, Y. Chen and Y. Wang, Adv Mater, 2017, 29. https://doi.org/10.1002/adma.201605838

[12] F. Cheng and J. Chen, Chem Soc Rev, 2012, 41, 2172-2192. https://doi.org/10.1039/c1cs15228a

[13] Y. Lee, J. Suntivich, K. J. May, E. E. Perry and Y. Shao-Horn, J Phys Chem Lett, 2012, 3, 399-404. https://doi.org/10.1021/jz2016507

[14] X. Zou and Y. Zhang, Chem. Soc. Rev., 2015, 44, 5148-5180. https://doi.org/10.1039/C4CS00448E

[15] C. G. Morales-Guio, L.-A. Stern and X. Hu, Chem. Soc. Rev., 2014, 43, 6555-6569. https://doi.org/10.1039/C3CS60468C

[16] S. Jiao, X. Fu, S. Wang and Y. Zhao, Energy Environ. Sci., 2021, 14, 1722-1770. https://doi.org/10.1039/D0EE03635H

[17] Q. Shi, C. Zhu, D. Du and Y. Lin, Chem. Soc. Rev., 2019, 48, 3181-3192. https://doi.org/10.1039/C8CS00671G

[18] J. Bonde, P. G. Moses, T. F. Jaramillo, J. K. Nørskov and I. Chorkendorff, Faraday Discuss., 2009, 140, 219-231. https://doi.org/10.1039/B803857K

[19] V. Vij, S. Sultan, A. M. Harzandi, A. Meena, J. N. Tiwari, W.-G. Lee, T. Yoon and K. S. Kim, ACS Catal., 2017, 7, 7196-7225. https://doi.org/10.1021/acscatal.7b01800

[20] Y. Zhang, Q. Zhou, J. Zhu, Q. Yan, S. X. Dou and W. Sun, Adv. Funct. Mater., 2017, 27, 1702317. https://doi.org/10.1002/adfm.201702317

[21] J. Duan, S. Chen and C. Zhao, Nat. Commun., 2017, 8, 15341. https://doi.org/10.1038/ncomms15341

[22] L. Han, S. Dong and E. Wang, Adv. Mater., 2016, 28, 9266-9291. https://doi.org/10.1002/adma.201602270

[23] S. Anantharaj, S. R. Ede, K. Sakthikumar, K. Karthick, S. Mishra and S. Kundu, ACS Catalysis, 2016, 6, 8069-8097. https://doi.org/10.1021/acscatal.6b02479

[24] L. Han, S. Dong and E. Wang, Adv Mater, 2016, 28, 9266-9291. https://doi.org/10.1002/adma.201602270

[25] Y. Yang, K. Zhang, H. Lin, X. Li, H. C. Chan, L. Yang and Q. Gao, ACS Catal., 2017, 7, 2357-2366. https://doi.org/10.1021/acscatal.6b03192

[26] J. Zhang, D. Zhang, R. Zhang, N. Zhang, C. Cui, J. Zhang, B. Jiang, B. Yuan, T. Wang, H. Xie and Q. Li, ACS Applied Energy Materials, 2018, 1, 495-502. https://doi.org/10.1021/acsaem.7b00099

[27] G. Sheng, J. Chen, Y. Li, H. Ye, Z. Hu, X. Z. Fu, R. Sun, W. Huang and C. P. Wong, ACS Appl Mater Interfaces, 2018, 10, 22248-22256. https://doi.org/10.1021/acsami.8b05427

[28] Z. Wang, H. Liu, R. Ge, X. Ren, J. Ren, D. Yang, L. Zhang and X. Sun, ACS Catalysis, 2018, 8, 2236-2241. https://doi.org/10.1021/acscatal.7b03594

[29] J. G. Wang, W. Hua, M. Li, H. Liu, M. Shao and B. Wei, ACS Appl Mater Interfaces, 2018, DOI: 10.1021/acsami.8b11576. https://doi.org/10.1021/acsami.8b11576

[30] H.-H. Zou, C.-Z. Yuan, H.-Y. Zou, T.-Y. Cheang, S.-J. Zhao, U. Y. Qazi, S.-L. Zhong, L. Wang and A.-W. Xu, Catalysis Science & Technology, 2017, 7, 1549-1555. https://doi.org/10.1039/C7CY00035A

[31] L. He, B. Cui, B. Hu, J. Liu, K. Tian, M. Wang, Y. Song, S. Fang, Z. Zhang and Q. Jia, ACS Applied Energy Materials, 2018, 1, 3915-3928. https://doi.org/10.1021/acsaem.8b00663

[32] P. Ganesan, M. Prabu, J. Sanetuntikul and S. Shanmugam, ACS Catal., 2015, 5, 3625-3637. https://doi.org/10.1021/acscatal.5b00154

[33] J. Wang, H.-x. Zhong, Z.-l. Wang, F.-l. Meng and X.-b. Zhang, ACS Nano, 2016, 10, 2342-2348. https://doi.org/10.1021/acsnano.5b07126

[34] S. Dou, L. Tao, J. Huo, S. Wang and L. Dai, Energy Enviorn. Sci., 2016, 9, 1320-1326. https://doi.org/10.1039/C6EE00054A

[35] T. Liu, Y. Liang, Q. Liu, X. Sun, Y. He and A. M. Asiri, Electrochem. Commun., 2015, 60, 92-96. https://doi.org/10.1016/j.elecom.2015.08.011

[36] Y. Surendranath, D. A. Lutterman, Y. Liu and D. G. Nocera, J. Am. Chem. Soc., 2012, 134, 6326-6336. https://doi.org/10.1021/ja3000084

[37] M. S. Faber, R. Dziedzic, M. A. Lukowski, N. S. Kaiser, Q. Ding and S. Jin, J. Am. Chem. Soc., 2014, 136, 10053-10061. https://doi.org/10.1021/ja504099w

[38] S. Wan, Y. Liu, G.-D. Li, X. Li, D. Wang and X. Zou, Catal. Sci. Technol., 2016, 6, 4545-4553. https://doi.org/10.1039/C5CY02292D

[39] Y. Liu, C. Xiao, M. Lyu, Y. Lin, W. Cai, P. Huang, W. Tong, Y. Zou and Y. Xie, Angew. Chem. Int. Ed., 2015, 54, 11231-11235. https://doi.org/10.1002/anie.201505320

[40] M. Liu and J. Li, ACS Appl. Mater. Interfaces, 2016, 8, 2158-2165. https://doi.org/10.1021/acsami.5b10727

[41] J. Chang, Y. Xiao, M. Xiao, J. Ge, C. Liu and W. Xing, ACS Catal., 2015, 5, 6874-6878. https://doi.org/10.1021/acscatal.5b02076

[42] A. Dutta, A. K. Samantara, S. K. Dutta, B. K. Jena and N. Pradhan, ACS Energy Letters, 2016, 1, 169-174. https://doi.org/10.1021/acsenergylett.6b00144

[43] E. J. Popczun, C. G. Read, C. W. Roske, N. S. Lewis and R. E. Schaak, Angewandte Chemie, 2014, 126, 5531-5534. https://doi.org/10.1002/ange.201402646

[44] S. Anantharaj, P. N. Reddy and S. Kundu, Inorg. Chem., 2017, 56, 1742-1756. https://doi.org/10.1021/acs.inorgchem.6b02929

[45] F. Du, Y. Zhang, H. He, T. Li, G. Wen, Y. Zhou and Z. Zou, J. Power Sources, 2019, 431, 182-188. https://doi.org/10.1016/j.jpowsour.2019.05.063

[46] D. Kong, J. J. Cha, H. Wang, H. R. Lee and Y. Cui, Energy Enviorn. Sci., 2013, 6, 3553-3558. https://doi.org/10.1039/c3ee42413h

[47] M. S. Faber, M. A. Lukowski, Q. Ding, N. S. Kaiser and S. Jin, The Journal of Physical Chemistry C, 2014, 118, 21347-21356. https://doi.org/10.1021/jp506288w

[48] X.-Y. Yu, L. Yu, H. B. Wu and X. W. Lou, Angew. Chem. Int. Ed., 2015, 54, 5331-5335. https://doi.org/10.1002/anie.201500267

[49] M. Ledendecker, S. Krick Calderón, C. Papp, H.-P. Steinrück, M. Antonietti and M. Shalom, Angew. Chem. Int. Ed., 2015, 54, 12361-12365. https://doi.org/10.1002/anie.201502438

[50] L.-A. Stern, L. Feng, F. Song and X. Hu, Energy Enviorn. Sci., 2015, 8, 2347-2351. https://doi.org/10.1039/C5EE01155H

[51] E. J. Popczun, J. R. McKone, C. G. Read, A. J. Biacchi, A. M. Wiltrout, N. S. Lewis and R. E. Schaak, J. Am. Chem. Soc., 2013, 135, 9267-9270. https://doi.org/10.1021/ja403440e

[52] A. Dutta and N. Pradhan, J. Phys. Chem. Lett., 2017, 8, 144-152. https://doi.org/10.1021/acs.jpclett.6b02249

[53] Z. Wu, X. Li, W. Liu, Y. Zhong, Q. Gan, X. Li and H. Wang, ACS Catal., 2017, 7, 4026-4032. https://doi.org/10.1021/acscatal.7b00466

[54] D. Li, H. Baydoun, B. Kulikowski and S. L. Brock, Chem. Mater., 2017, 29, 3048-3054. https://doi.org/10.1021/acs.chemmater.7b00055

[55] R. Zhang, X. Wang, S. Yu, T. Wen, X. Zhu, F. Yang, X. Sun, X. Wang and W. Hu, Adv Mater, 2017, 29. https://doi.org/10.1002/adma.201770059

[56] X. Y. Yu, Y. Feng, Y. Jeon, B. Guan, X. W. Lou and U. Paik, Adv Mater, 2016, 28, 9006-9011. https://doi.org/10.1002/adma.201601188

[57] Z. C. Liu, G. Zhang, K. Zhang, H. J. Liu and J. H. Qu, ACS Sustainable Chemistry & Engineering, 2018, 6, 7206-7211. https://doi.org/10.1021/acssuschemeng.8b00471

[58] K. W. Liu, C. L. Zhang, Y. D. Sun, G. H. Zhang, X. C. She, F. Zou, H. C. Zhang, Z. W. Wu, E. C. Wegener, C. J. Taubert, J. T. Miller, Z. M. Peng and Y. Zhu, ACS Nano, 2018, 12, 158-167. https://doi.org/10.1021/acsnano.7b04646

[59] L. M. Cao, Y. W. Hu, S. F. Tang, A. Iljin, J. W. Wang, Z. M. Zhang and T. B. Lu, Adv Sci (Weinh), 2018, 5, 1800949. https://doi.org/10.1002/advs.201800949

[60] Y. Li, H. Zhang, M. Jiang, Q. Zhang, P. He and X. Sun, Advanced Functional Materials, 2017, 27, 1702513. https://doi.org/10.1002/adfm.201702513

[61] Y. Pan, Y. Liu, Y. Lin and C. Liu, ACS Appl. Mater. Interfaces, 2016, 8, 13890-13901. https://doi.org/10.1021/acsami.6b02023

[62] J. Yang, G. Zhu, Y. Liu, J. Xia, Z. Ji, X. Shen and S. Wu, Adv. Funct. Mater., 2016, 26, 4712-4721. https://doi.org/10.1002/adfm.201600674

[63] X.-Y. Yu, Y. Feng, Y. Jeon, B. Guan, X. W. Lou and U. Paik, Adv. Mater., 2016, 28, 9006-9011. https://doi.org/10.1002/adma.201601188

[64] P. He, X.-Y. Yu and X. W. Lou, Angew. Chem. Int. Ed., 2017, 56, 3897-3900. https://doi.org/10.1002/anie.201612635

[65] L. Yu, L. Zhang, H. B. Wu and X. W. Lou, Angew. Chem. Int. Ed., 2014, 53, 3711-3714. https://doi.org/10.1002/anie.201400226

[66] L. Shen, L. Yu, H. B. Wu, X.-Y. Yu, X. Zhang and X. W. Lou, Nat. Commun., 2015, 6, 6694. https://doi.org/10.1038/ncomms7694

[67] Miguel Cabán-Acevedo, Michael L. Stone, J. R. Schmidt, Joseph G. Thomas, Qi Ding, Hung-Chih Chang, Meng-Lin Tsai, Jr-Hau He and S. Jin, Nat. Mater., 2015, 14, 1245-1253. https://doi.org/10.1038/nmat4410

[68] P. Wang, Z. Pu, Y. Li, L. Wu, Z. Tu, M. Jiang, Z. Kou, I. S. Amiinu and S. Mu, ACS Appl. Mater. Interfaces, 2017, 9, 26001-26007. https://doi.org/10.1021/acsami.7b06305

[69] X. Feng, Q. Jiao, H. Cui, M. Yin, Q. Li, Y. Zhao, H. Li, W. Zhou and C. Feng, ACS Appl. Mater. Interfaces, 2018, 10, 29521-29531. https://doi.org/10.1021/acsami.8b08547

[70] J. Li, M. Yan, X. Zhou, Z.-Q. Huang, Z. Xia, C.-R. Chang, Y. Ma and Y. Qu, Adv. Funct. Mater., 2016, 26, 6785-6796. https://doi.org/10.1002/adfm.201601420

[71] R. Zhang, X. Wang, S. Yu, T. Wen, X. Zhu, F. Yang, X. Sun, X. Wang and W. Hu, Adv. Mater., 2017, 29, 1605502-n/a. https://doi.org/10.1002/adma.201605502

[72] K. Liu, C. Zhang, Y. Sun, G. Zhang, X. Shen, F. Zou, H. Zhang, Z. Wu, E. C. Wegener, C. J. Taubert, J. T. Miller, Z. Peng and Y. Zhu, ACS Nano, 2018, 12, 158-167. https://doi.org/10.1021/acsnano.7b04646

[73] C. G. Read, J. F. Callejas, C. F. Holder and R. E. Schaak, ACS Appl. Mater. Interfaces, 2016, 8, 12798-12803. https://doi.org/10.1021/acsami.6b02352

[74] Y. Guo, J. Tang, Z. Wang, Y. Sugahara and Y. Yamauchi, Small, 2018, 14, 1802442. https://doi.org/10.1002/smll.201802442

[75] H. Liang, A. N. Gandi, D. H. Anjum, X. Wang, U. Schwingenschlögl and H. N. Alshareef, Nano Lett., 2016, 16, 7718-7725. https://doi.org/10.1021/acs.nanolett.6b03803

[76] N. Jiang, B. You, M. Sheng and Y. Sun, Angew. Chem. Int. Ed., 2015, 54, 6251-6254. https://doi.org/10.1002/anie.201501616

[77] D. Xiong, X. Wang, W. Li and L. Liu, Chem. Commun., 2016, 52, 8711-8714. https://doi.org/10.1039/C6CC04151E

[78] T. Yang, L. Yin, M. He, W. Wei, G. Cao, X. Ding, Y. Wang, Z. Zhao, T. Yu, H. Zhao and D. Zhang, Chem. Commun., 2019, 55, 14343-14346. https://doi.org/10.1039/C9CC06244K

[79] T. Yang, Y. Wang, W. Wei, X. Ding, M. He, T. Yu, H. Zhao and D. Zhang, Nanoscale, 2019, 11, 23206-23216. https://doi.org/10.1039/C9NR07235G

[80] Y. Li, H. Zhang, T. Xu, Z. Lu, X. Wu, P. Wan, X. Sun and L. Jiang, Advanced Functional Materials, 2015, 25, 1737-1744. https://doi.org/10.1002/adfm.201404250

[81] L. Zhang, K. Xiong, S. Chen, L. Li, Z. Deng and Z. Wei, Journal of Power Sources, 2015, 274, 114-120. https://doi.org/10.1016/j.jpowsour.2014.10.038

[82] L. Han, X. Y. Yu and X. W. Lou, Adv Mater, 2016, 28, 4601-4605. https://doi.org/10.1002/adma.201506315

[83] F. L. Li, Q. Shao, X. Huang and J. P. Lang, Angew Chem Int Ed Engl, 2018, 57, 1888-1892. https://doi.org/10.1002/anie.201711376

[84] X. L. Wu, S. Han, D. H. He, C. L. Yu, C. J. Lei, W. Liu, G. K. Zheng, X. W. Zhang and L. C. Lei, ACS Sustainable Chemistry & Engineering, 2018, DOI: 10.1021/.

[85] X. Hou, Y. Zhang, Q. Dong, Y. Hong, Y. Liu, W. Wang, J. Shao, W. Si and X. Dong, ACS Applied Energy Materials, 2018, 1, 3513-3520. https://doi.org/10.1021/acsaem.8b00773

[86] X. Y. Yu, L. Yu, H. B. Wu and X. W. Lou, Angew Chem Int Ed Engl, 2015, 54, 5331-5335. https://doi.org/10.1002/anie.201500267

[87] J. Li, S. Q. Lu, H. L. Huang, D. H. Liu, Z. B. Zhuang and C. L. Zhong, ACS Sustainable Chemistry & Engineering, 2018, 6, 10021-10029. https://doi.org/10.1021/acssuschemeng.8b01332

[88] L. Yan, L. Cao, P. Dai, X. Gu, D. Liu, L. Li, Y. Wang and X. Zhao, Advanced Functional Materials, 2017, 27, 1703455. https://doi.org/10.1002/adfm.201703455

[89] K. Ao, J. Dong, C. Fan, D. Wang, Y. Cai, D. Li, F. Huang and Q. Wei, ACS Sustainable Chemistry & Engineering, 2018, 6, 10952-10959. https://doi.org/10.1021/acssuschemeng.8b02343

[90] W. Wang, X. Xu, W. Zhou and Z. Shao, Adv Sci (Weinh), 2017, 4, 1600371. https://doi.org/10.1002/advs.201600371

[91] Y. Guo, J. Tang, Z. Wang, Y. Sugahara and Y. Yamauchi, Small, 2018, 14, e1802442. https://doi.org/10.1002/smll.201802442

[92] W. Ahn, M. G. Park, D. U. Lee, M. H. Seo, G. Jiang, Z. P. Cano, F. M. Hassan and Z. Chen, Advanced Functional Materials, 2018, 28, 1802129. https://doi.org/10.1002/adfm.201802129

[93] C. Xuan, J. Wang, W. Xia, Z. Peng, Z. Wu, W. Lei, K. Xia, H. L. Xin and D. Wang, ACS Appl Mater Interfaces, 2017, 9, 26134-26142. https://doi.org/10.1021/acsami.7b08560

[94] Z. Wu, J. Guo, J. Wang, R. Liu, W. Xiao, C. Xuan, K. Xia and D. Wang, ACS Appl Mater Interfaces, 2017, 9, 5288-5294. https://doi.org/10.1021/acsami.6b15244

[95] Y. Li and C. Zhao, Chemistry of Materials, 2016, 28, 5659-5666. https://doi.org/10.1021/acs.chemmater.6b01522

[96] J. Hao, W. Yang, Z. Zhang and J. Tang, Nanoscale, 2015, 7, 11055-11062. https://doi.org/10.1039/C5NR01955A

[97] X. Xiao, C.T. He, S. Zhao, J. Li, W. Lin, Z. Yuan, Q. Zhang, S. Wang, L. Dai and D. Yu, Energy & Environmental Science, 2017, 10, 893-899. https://doi.org/10.1039/C6EE03145E

Received on 03-05-2023 Accepted on 25-05-2023 Published on 26-05-2023

DOI: https://doi.org/10.31875/2410-4701.2023.10.05